Proceedings of the 9th U.S. National and 10th Canadian Conference on Earthquake Engineering
Compte Rendu de la 9ième Conférence Nationale Américaine et
10ième Conférence Canadienne de Génie Parasismique
July 25-29, 2010, Toronto, Ontario, Canada • Paper No 1068

EXPERIMENTAL TESTS ON CYCLIC BEAM-COLUMN INTERACTION STRENGTH OF CONCRETE-FILLED STEEL TUBES

Tiziano Perea[1], Roberto T. Leon[2], Mark D. Denavit[3] and Jerome F. Hajjar[4]

ABSTRACT

This paper presents selected experimental results on 18 tests on circular and rectangular concrete-filled steel tubes (CFT) subjected to cyclic loads. The selected test matrix in this experimental study is unique for the size and slenderness of the specimens, which fill gaps found in the available experimental CFT databases. Different steel tube shapes with high slender both for width-thickness ratios and lengths are the main characteristics of the CFT test matrix tested in this research. These CFT specimens were subjected to different load cases (i.e. internal pressure due to filling, critical load, cyclic uniaxial and biaxial bending with different axial force levels, and finally torsion). The load protocol addresses the measurement of the column critical load and the determination of the beam-column P-M interaction diagram, both accounting for the stability reduction. In addition, both the stiffness and strength degradation and the progression of local buckling are evaluated through a load case with incremental cyclic top lateral displacement. The tests confirmed the extreme toughness and strength of composite concrete-filled beam-columns.

Introduction

Due the synergy effects in composite concrete-steel beam-columns, these elements are known as one of the toughest and most efficient structural members for use in seismic design. In developing design provisions for such composite columns for the 2005 Specification for Structural Steel Buildings (AISC, 2005), the senior authors noted that databases contained few if any tests on slender composite beam-columns (Leon at. al, 2007; Leon and Hajjar, 2008). To address this deficiency in the short term and from the design standpoint, the Specification assumed that slender composite beam-column could be modeled as steel sections with an equivalent moment of inertia. In the longer term, a series of advanced tests on 18 concrete-filled (CFT) slender columns has been completed to address a number of outstanding issues, primarily how the stiffness of the members evolves with different combinations of axial loads and moments for slender elements. In this test series, a number of the columns were so slender as to challenge the capabilities of the advanced control systems and loading fixtures used.

[1] Graduate Research Assistant, Dept. of Civil Engineering, Georgia Institute of Technology, Atlanta, GA 30332
[2] Professor, Dept. of Civil and Environmental Engineering, Georgia Institute of Technology, Atlanta, GA 30332
[3] Graduate Research Assistant, Dept. of Civil Engineering, University of Illinois at Urbana-Champaign, IL 61801
[4] Professor, Dept. of Civil Engineering, University of Illinois at Urbana-Champaign, IL 61801

This paper describes the test series in detail and presents some of the experimental test results. Characterization of the experimental behavior is a key to the calibration of mixed-formulation models to be used to properly model the performance of these beam-columns in real structures.

Experimental Program

Test Matrix

The test matrix selected for these tests aims to fill gaps found in the available experimental databases (Leon et al., 2005; Goode et al., 2006). Eighteen specimens with different steel tube shapes, width-thickness ratios (*h/t*, *D/t*) and lengths (*L*), and filled with normal and high strength concrete were constructed. The test matrix is shown in Table 1 along with the nominal material strengths. The 2005 Specification allows a maximum *D/t* of 103.6 for circular tubes and a maximum *h/t* of 56.7 for rectangular tubes, so some of the larger tubes shown in Table 1 are very near or above those limits. Typical specimens placed at the testing equipment are shown in Figure 1.

Table 1. Test Matrix

Specimen Name	*L* (ft)	Steel section HSS D x t	F_y (ksi)	f_c' (ksi)	*D/t*
C12-18-05	18	HSS12.75X0.25	42	5	55
C12-18-12	18	HSS12.75X0.25	42	12	55
C12-26-05	26	HSS12.75X0.25	42	5	55
C12-26-12	26	HSS12.75X0.25	42	12	55
C20-18-05	18	HSS20x0.25	42	5	86
C20-18-12	18	HSS20x0.25	42	12	86
C20-26-05	26	HSS20x0.25	42	5	86
C20-26-12	26	HSS20x0.25	42	12	86
RW-18-05	18	HSS20x12x0.25	46	5	67
RW-18-12	18	HSS20x12x0.25	46	12	67
RW-26-05	26	HSS20x12x0.25	46	5	67
RW-26-12	26	HSS20x12x0.25	46	12	67
RS-18-05	18	HSS20x12x0.25	46	5	67
RS-18-12	18	HSS20x12x0.25	46	12	67
RS-26-05	26	HSS20x12x0.25	46	5	67
RS-26-12	26	HSS20x12x0.25	46	12	67
C5-18-05	18	HSS5.563x0.134	42	5	45
C5-26-12	26	HSS5.563x0.134	42	12	45

The specimens were fabricated from A500 Grade B material. Actual yield strengths measured from coupon tests ranged from 46.1 to 55.6 ksi and 53.0 to 53.9 ksi for the circular and rectangular tubes, respectively. The infill concrete was self-consolidating (SCC). The compression strength for the lower strength mix (nominally 5 ksi) ranged from 5.5 to 8.9 ksi from cylinder tests conducted at the time of testing. The strength for the higher strength mix (nominally 12 ksi), which contained silica fume and fly ash, ranged from 11.3 to 13.8 ksi at time of testing. Thick plates were welded at either end of the specimen. The thicker bottom plate

connected the specimen to the strong floor (to simulate a fixed base) and the thinner top plate to the crosshead (simulating a roller, pinned or fixed condition). Finite element analyses were conducted to check the strength of the base plates, the welds and the entre connection.

Testing System

These full-scale specimens were conducted on the Multi-Axial Sub-assemblage Testing (MAST) laboratory, a NEES facility at the University of Minnesota. The MAST system (Figure 1) consist of a stiff steel crosshead connected to 4 vertical actuators (with a load capacity of 330 kips and stroke of ±20 inches each) and 2 actuators in each horizontal axis (with a load capacity of 440 kips and stroke of ±20 inches each). All of the actuators are pin-pin connected, with the crosshead free-floating, giving the MAST system the capability of controlling the top 6 DOFs with a maximum capacity of P_z=1320 kips in vertical force, F_x=F_y=880 kips in shear, and a maximum stroke of ±20 in for horizontal and vertical displacements. The vertical opening of the MAST system can be adjusted between 18 and 28 feet. The MTS controller is very similar to those used to control a 6 DOF shake table installation.

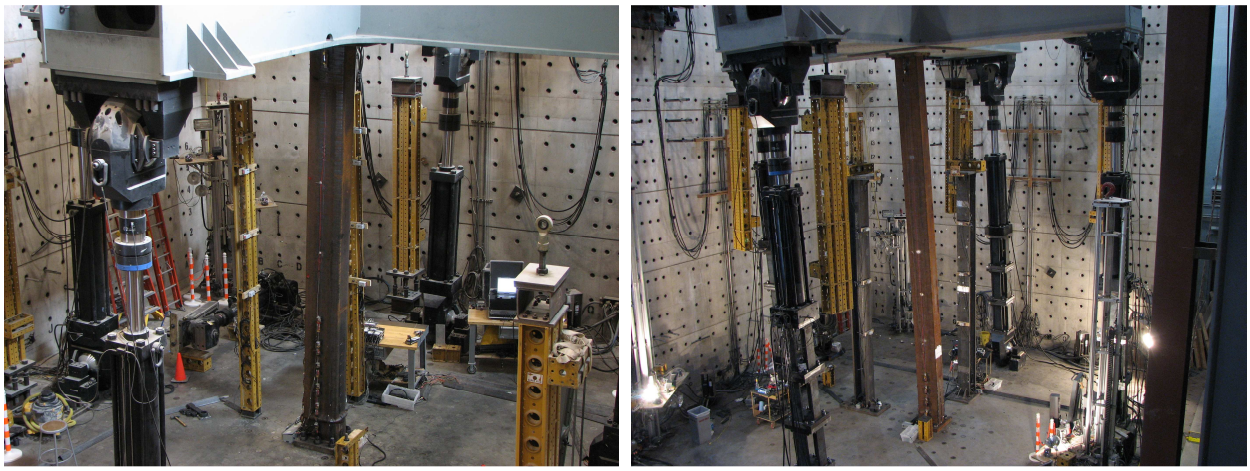

(a) Specimen RW-18-12 (b) Specimen RW-26-12

Figure 1. MAST system and CFT specimens

Instrumentation

The specimens were extensively instrumented with redundant measuring systems in order to characterize the moment-curvature behavior of the critical cross-sections near the bottom of the specimens. In addition, as the specimens were designed to be loaded primarily as fixed-free cantilever columns in order to increase their slenderness, a large number of displacement transducers were used to track lateral deformations.

The primary aim of the tests was to track the changes in effective stiffness along the length of the beam-column as the loading progressed. Thus, arrays of strain gages, LVDTs and LEDs for a Metris K600 DDM laser system were placed at close intervals near the critical sections. The instrumentation was also designed to limit the loss of data due to the local buckling that was expected to form at the latter stages of the testing. Typical channel counts included 8 loads cells, 18 LVDTs, 5 string pots, 30 strain gages and 40 LEDs. In addition, extensive video and photographic data was collected during each test.

Loading Protocol

The CFT specimens were subjected to a complex load protocol consisting of several distinct load cases (LC), each intended to addresses the main objectives of the test series:

- *Buckling load of the CFT columns accounting for the effectiveness of the composite stiffness on the stability effects with given boundary conditions*. This was LC1, which applied incremental compression through vertical displacement control (with all the other DOFs at the top set to zero load) until instability arose.

- *Determination of the maximum flexural capacity under different gravity conditions to allow the construction of P-M interaction diagram for CFT beam-columns.* This was LC2, in which increasing cyclic unidirectional lateral displacements were applied under constant gravity force until the peak and softening were found. These tests were repeated at multiple axial load levels.

- *Evaluation of the concrete confinement, the progression of steel local buckling and its effects on the composite stiffness, ductility and strength degradation.* This was LC3, where multidirectional lateral displacements with constant gravity force were applied. Several lateral displacement patterns, including "diamond" and "figure 8" shapes were used.

- *Evolution of the flexural (EI_{eff}) and torsional (GJ_{eff}) stiffness*. This was LC4 in which monotonic uniaxial or biaxial displacements to the maximum system stroke were applied. This was followed in several specimens by twisting to obtain data on torsional performance.

Initial Test Configuration

The pretest setup in the CCFT specimens for each tests had the following sequence:

- Columns were instrumented and strains monitored during casting to measure the effects of the hydrostatic pressure of the wet concrete; appreciable strains and bulging near the bottom was evident for the RCFTs.

- The out-of-plumbness and the out-of-straightness with respect to the X and Y axes were measured using both a plum bob and a theodolite. Initial imperfections for the column, which often were in excess of $L/500$; this was not surprising as the columns were long.

- Offsets for crosshead forces were taken. With all the instrumentation connected to the DAQ, data started being recorded with offsets for the crosshead forces only. At the starting point, the crosshead forces and moments were zero, with some noise level ($F_z \approx \pm$ 0.32 kip, $F_x = F_y \approx \pm$ 0.22 kip, $M_x = M_y \approx \pm$ 2.2 kip-ft, $M_z \approx \pm$ 2.9 kip-ft).

- Final connection and tensioning of the top plate to the crosshead. Threaded rods were tensioned until 60% of the yield stress was reached. The connection process created forces and moments that were monitored and recorded.

- Removal of the forces and moments induced during the connection. The crosshead was moved until the system came back to the initial state of zero forces and moments. The data taken during this process was named LC0 and served as the baseline for the test.

- Rest of the offsets taken. Once in the initial state, offsets for the crosshead position and offsets for the entire instrumentation were taken. Initial strains from the gages and relative displacements from the LVDTs were then set to zero within the resolution range.

Experimental Results

Wet Concrete Effects

As described before, longitudinal and transverse strain data was taken during the pouring of concrete in order to evaluate the effects of the wet concrete. Analytical closed-form solutions and FE analyses of the steel tubes under hydrostatic pressures coming from the wet concrete were performed for the specimens. These analyses showed a very low strain and negligible deflection for the circular tubes. However, the level of strains and lateral deflection were considerable for the rectangular tubes, where the calculated hydrostatic pressure resulted in up to 80% of the yield stress and ¼" of expansion at about 2 feet from the base for the longer RCFTs. In order to reduce this amount of expansion in the rectangular steel tubes, lateral confinement frames were placed every foot for the bottom 5 feet. This lateral frames consisted of two angles placed on the 20 inches walls and tied with threaded rods on each side along the 12 inches walls. This reinforcement were used in all the RCFTs, except in the RW-18-5 specimen, were the lateral strains were measured in a non-restrained conditioned.

Table 2 shows the predicted and the measured transverse strain and expansion in the rectangular steel tubes under the hydrostatic pressure induced by the wet concrete. The analytical prediction was obtained for the non-restrained condition; the experimental values shown correspond to the restrained condition, except for the 18 feet steel tube where the non-restrained maximum transverse strain was also measured. A comparison between the experimental lateral strains obtained in the steel tubes with a restrained and a non-restrained condition is shown in Figure 2(a). As shown in these results, the lateral reinforcement reduced by about 50 to 65% the lateral strains that it was expected without this reinforcement. In addition, the expansion was also reduced by about a similar ratio.

The lateral reinforcement was removed once the concrete inside the steel tubes hardened. It was not surprising that for the RW-18-5 specimen, which did not have lateral reinforcement during the concrete casting, the deformations during casting led to a higher position of the local buckling during the test. As predicted for the non-restrained case, the maximum expansion located between 1.5 to 2.5 feet from the base induced an initial out-of-straightness in the steel walls, expansion that was also taken by the concrete once this hardened. This initial out-of-straightness grew rapidly once compressive and bending loads were applied. Figure 2(b) and Figure 2(c) show the specimens at the end of the load protocol test, contrasting the effects of the wet concrete pressure with and without lateral reinforcement in regards of the steel local buckling elevation.

Table 2. Maximum transverse strain due to the wet concrete pressure in RCFTs

L (ft)	Approach	Transverse Strain (x10^{-6})	Stress (ksi)	Expansion (in)
18	Analytical	800	23.2	0.167
	Experimental	728	21.1	$\approx 1/8$
	Experimental*	484	14.0	$\approx 1/16$
26	Analytical	1278	37.1	0.241
	Experimental*	706	20.5	$\approx 1/8$

* Maximum experimental value measured in the specimen with lateral reinforcement

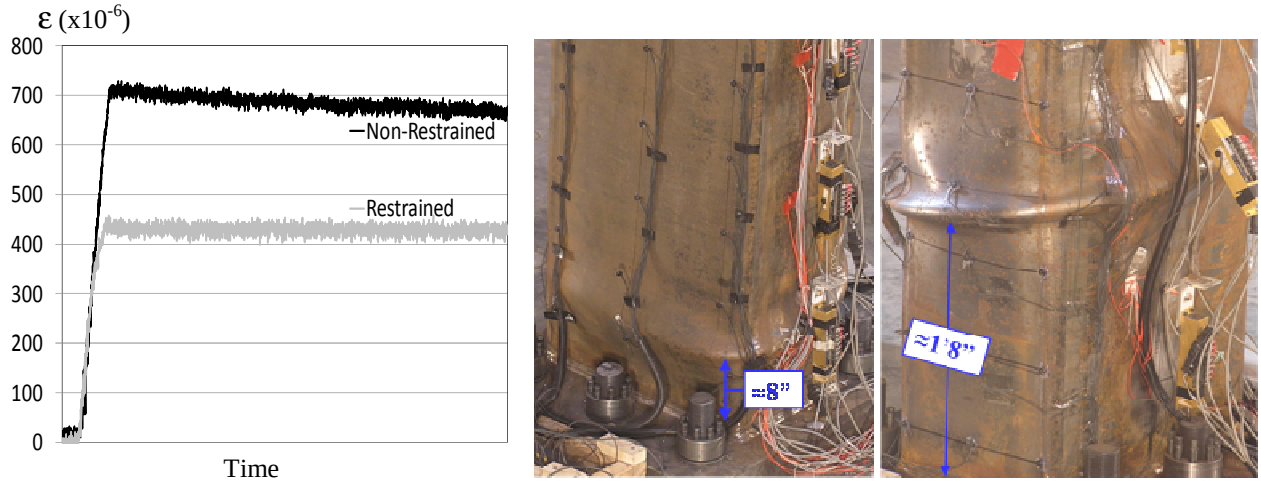

(a) Transverse strain vs. time at pouring (b) Restrained RCFT after testing (c) Non-restrained after testing

Figure 2. Transverse strains between restrained and non-restrained RCFTs during the concrete pouring and local buckling position at the end of the testing.

Experimental Critical Axial Load

The first load case was intended to determine the critical axial load. Most specimens had forces and bending moments controlled so they were hold at zero value at the top (free top, K=2); some specimens were controlled in either zero lateral force – fixed rotation (K=0.7), fixed lateral force – fixed rotation (K=0.5), or both.

Table 3 summarizes the results of the maximum experimental compressive load (P_{exp}) supported by each specimen. In this table, the calculated buckling critical axial load (P_n) with the AISC 2005 Specification for each specimen is also compared. Figure 3 shows the loading branch vs. the drift obtained for this load case for the specimens of the C20 and RW series.

Differences between the critical values were expected due to variation in the initial imperfection between real and ideal conditions (Δ_o=L/500 for K=2 implicit in AISC-05). However, high differences were obtained in some cases due to additional frictional forces coming from the actuators. These additional forces are not negligible in some cases, where the boundary conditions can be changed and thus the critical axial load. Analytical determination of the critical axial loads with the experimental boundary conditions and accounting for the addition frictional forces are described by Leon et al. (2009) and by Denavit et al. (2010).

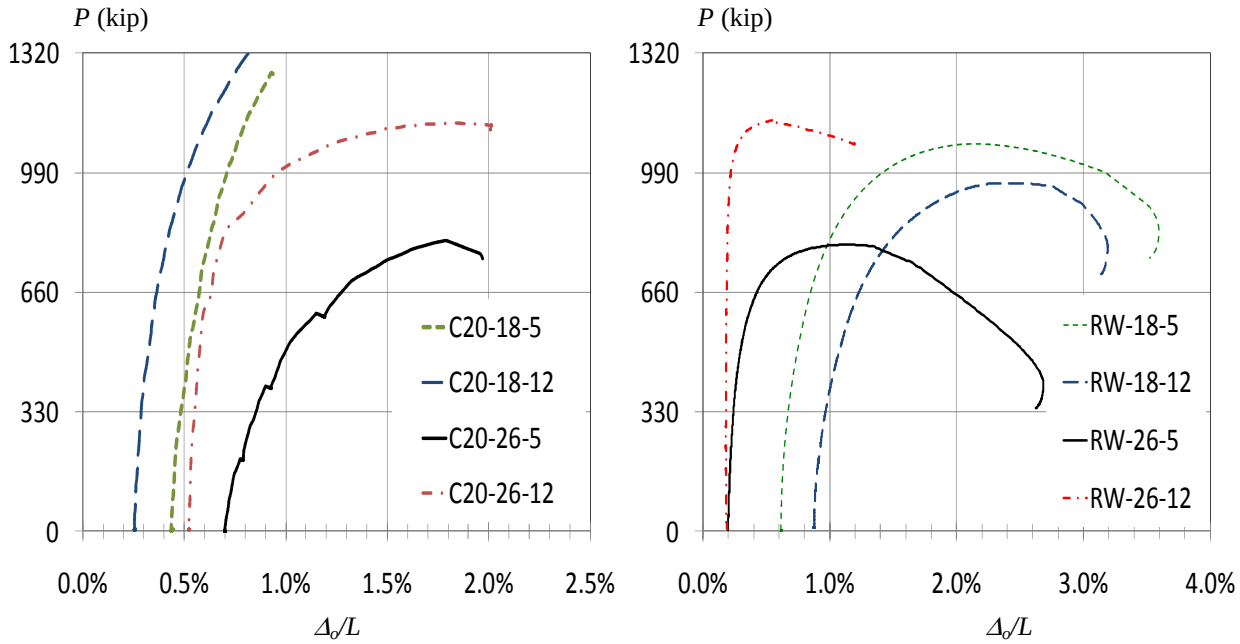

(a) Circular CFT, 20" diameter (b) Rectangular CFT, weak axis bending

Figure 3. Incremental compressive loading using fixed-free boundary conditions

Table 3 – Summary of the critical axial loads

Specimen name	f_c (ksi)	F_y (ksi)	L (ft, in)	Δ_o/L (%)	K -	λ -	P_n (kip)	P_{exp} (kip)
C12-18-05	5.6	48.9	18' $^1/_2$"	0.376	2	1.55	394	427
C12-18-12	13.2	48.9	18' $^1/_2$"	0.197	2	1.93	455	581
C12-26-05	7.9	48.9	26' 1"	0.322	2	2.43	200	362
C12-26-12	11.6	48.9	26' 1$^1/_2$"	0.205	2	2.70	212	386
C20-18-05	5.8	47.6	18' 1$^1/_2$"	0.438	2	1.05	1472	>1320 [1]
C20-18-12	13.2	47.6	18' 1$^7/_8$"	0.256	2	1.33	2115	>1320 [1]
C20-26-05	8.1	47.6	26' 2$^3/_4$"	0.701	2	1.67	945	802
C20-26-12	11.6	47.6	26' 2"	0.522	2	1.85	1026	1127
RW-18-05	5.9	53.0	18' 2"	0.621	2	1.38	938	1070
RW-18-12	13.3	53.0	18' 2$^5/_8$"	0.876	2	1.68	1079	961
RW-26-05	8.2	53.0	26' 1$^1/_4$"	0.286	2	2.13	486	791
RW-26-12	11.7	53.0	26' 1$^1/_4$"	0.424	2	2.33	514	1135
RS-18-05	5.9	53.0	18' 2"	0.212	2	0.88	1501	>1320 [1]
RS-18-12	13.3	53.0	18' 2$^5/_8$"	0.376	2	1.06	2163	>1320 [1]
RS-26-05	8.3	53.0	26' 1$^3/_4$"	0.216	2	1.36	1163	1320
RS-26-12	11.7	53.0	26' 1$^1/_2$"	0.881	2	1.48	1272	1125
C5-18-05	5.5	55.6	18' 1$^1/_2$"	N/A	0.5	0.90	168	163 [2]
C5-26-12	11.7	55.6	26' $^5/_8$"	N/A	0.5	1.52	138	141 [2]

(1) MAST axial capacity is 1320 kips. (2) Specimens loaded with double fixed boundary conditions.

Uniaxial and Biaxial Flexure

Uniaxial and biaxial bending with different levels of constant gravity load were applied monotonic and cyclically through moving the top in displacement control as shown in Figure 4. Each of this load cases pursues different goals, and each specimen was subjected to at least one uniaxial and one biaxial, with at least two different levels of constant gravity load. In some load cases, like those in Figures 4(a), 4(b), 4(d) and 4(e), the target displacements were those associated with (a) the softening in lateral force or, in other words, when the critical section reach the plastic moment (P^i-M_p^i); or (b) extraction of P-M_p values points toward in the determination of the P-M interaction surfaces of CFT beam-columns. Cyclic load cases, like those in Figures 4(a), 4(b), 4(c) and 4(e), had defined targets in terms of incremental drifts that lead to experimental determination of the strength and effective stiffness degradation, ductility and identification of limit states. As an example, the experimental responses of the specimen C20-26-12 to the uniaxial (as in Figure 4(b)) and biaxial (as in Figure 4(f)) are illustrated in Figure 5(a) and 5(b), respectively. Experimental response has improved the calibration of the material constitutive models for both steel and concrete, and the calibration of the non-linear beam-column response. Analytical determination of the beam-column response and its comparison with the experimental response is discussed in more detail in Denavit et al. (2010).

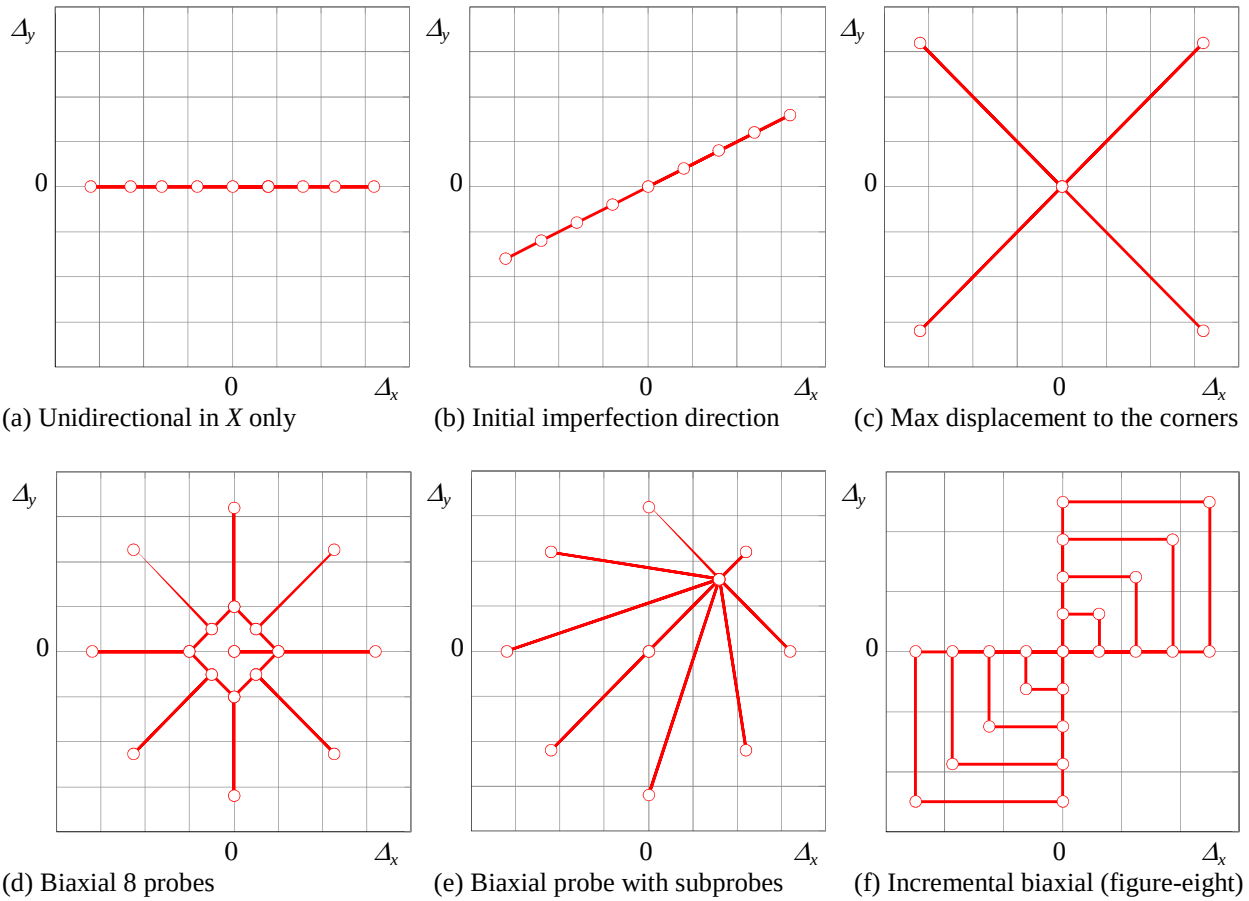

(a) Unidirectional in X only (b) Initial imperfection direction (c) Max displacement to the corners

(d) Biaxial 8 probes (e) Biaxial probe with subprobes (f) Incremental biaxial (figure-eight)

Figure 4. Top displacement patterns in uniaxial and biaxial load cases

(a) Uniaxial along the initial imperfection, P=400 (b) Incremental biaxial (figure-eight), P=200

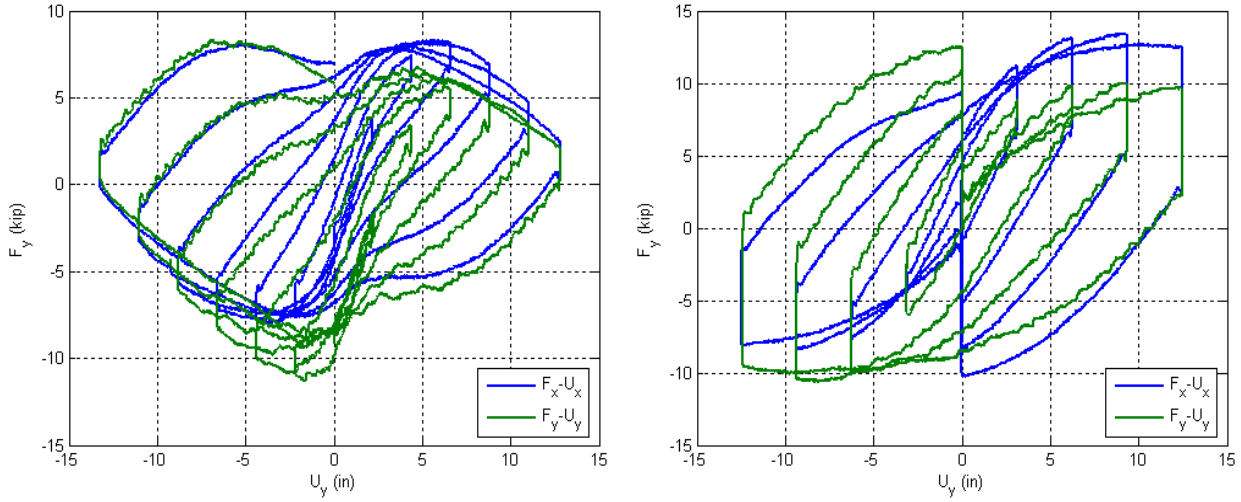

(i) Top force vs. top displacement

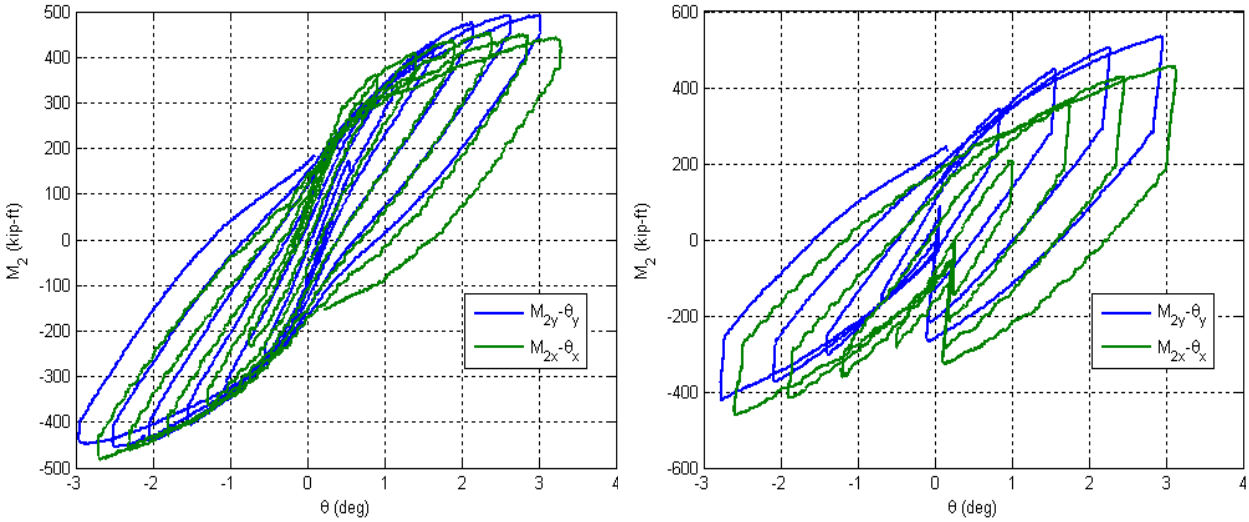

(ii) Base moment vs. top rotation (M_2-θ)

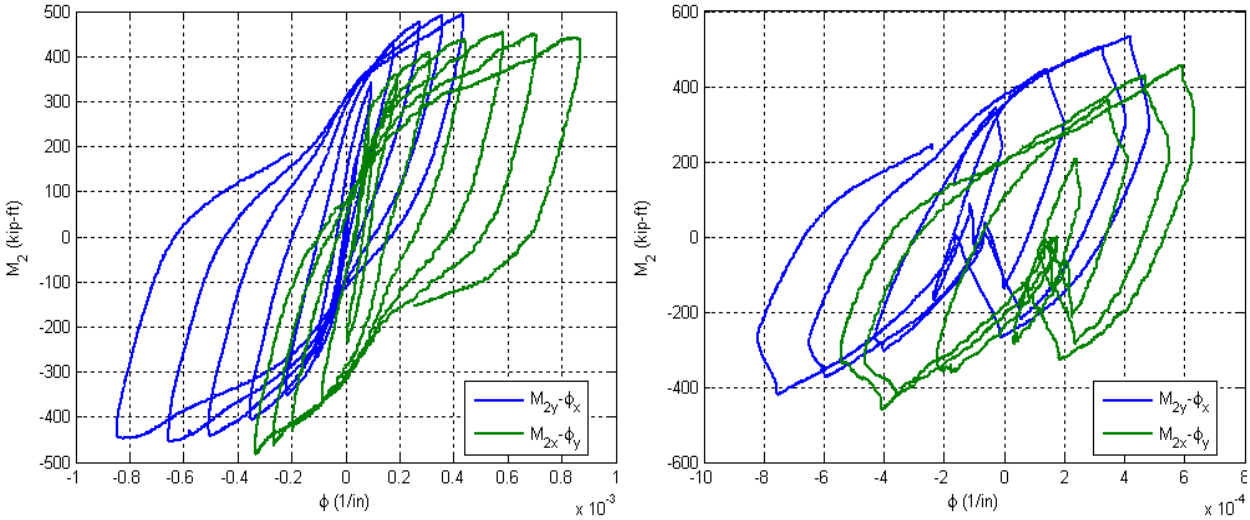

(iii) Base moment vs. base curvature (M_2-ϕ)

Figure 5. Cyclic histories for specimen C20-26-12

Conclusions

Test results from a comprehensive experimental research program of full-scale and slender circular and rectangular concrete-filled steel tubes (CFT) beam-columns were presented. These tests focused on the cyclic beam-column interaction strength of CFTs through a complex load protocol that addresses the experimental determination of the column critical axial load, the beam-column *P-M* interaction diagram, and the strength and the effective stiffness degradation for cyclic uniaxial and biaxial bending of beam-columns, all these accounting for the stability reduction. In addition, experimental evaluation of the wet concrete effects was conducted during the concrete pouring and during the load protocol tests. The experimental response obtained in the entire load protocol has allowed enhancing the calibration of the material constitutive models for both steel and concrete, and the calibration of mixed-formulation models that can be used to properly model the performance of CFT beam-columns in real structures.

Acknowledgments

The work described here is part of a NEESR project supported by the National Science Foundation under Grant No. CMMI-0619047, the American Institute of Steel Construction, the Georgia Institute of Technology, and the University of Illinois at Urbana-Champaign. In-kind funding was provided by Atlas Tube Inc. and LeJeune Steel Co. The valuable group effort of the MAST Personnel to the experimental program is greatly appreciated. Any opinions, findings, and conclusions expressed in this material are those of the authors and do not necessarily reflect the views of the National Science Foundation or other sponsors.

References

AISC, 2005. *Specifications for structural steel buildings*, ANSI/AISC 360-05, AISC, Chicago, Illinois.

Denavit, M. D., J. F. Hajjar, T. Perea, and R. T. Leon, 2010. Cyclic evolution of damage and beam-column interaction strength of concrete-filled steel tube beam-columns, *Proceedings of the 9th US National and 10th Canadian Conference on Earthquake Engineering*. Toronto, Canada.

Goode, C., 2007. *ASCCS database of concrete-filled steel tube columns*. ASCCS, http://web.ukonline.co.uk/asccs2/

Leon, R. T., and D. Kim, 2005. A database for composite columns, School of Civil and Environmental Engineering. *Report No. 1-05*, Georgia Institute of Technology. Atlanta, Georgia.

Leon, R. T., D. Kim, and J. F. Hajjar, 2007. Limit state response of composite columns and beam-columns; Part I: formulation of design provisions for the 2005 AISC specification, *Engineering Journal*, AISC, 44(4), 341–358.

Leon, R. T., and J. F. Hajjar, 2008. Limit state response of composite columns and beam-columns; Part II: Application of design provisions for the 2005 AISC specification, *Engineering Journal*, AISC, 45(1), 21-46.

Leon, R. T., T. Perea, J. F. Hajjar, and M. D. Denavit, 2009. Determination of buckling loads from triaxial load tests of slender concrete-filled tube beam-columns, *Proceeding of the 3rd International Conference on Advances in Experimental Structural Engineering*, San Francisco, California.